NASA/TM—2005-213599

A Study of Cavitation-Ignition Bubble Combustion

Quang-Viet Nguyen and David A. Jacqmin
Glenn Research Center, Cleveland, Ohio

August 2005

The NASA STI Program Office . . . in Profile

Since its founding, NASA has been dedicated to the advancement of aeronautics and space science. The NASA Scientific and Technical Information (STI) Program Office plays a key part in helping NASA maintain this important role.

The NASA STI Program Office is operated by Langley Research Center, the Lead Center for NASA's scientific and technical information. The NASA STI Program Office provides access to the NASA STI Database, the largest collection of aeronautical and space science STI in the world. The Program Office is also NASA's institutional mechanism for disseminating the results of its research and development activities. These results are published by NASA in the NASA STI Report Series, which includes the following report types:

- TECHNICAL PUBLICATION. Reports of completed research or a major significant phase of research that present the results of NASA programs and include extensive data or theoretical analysis. Includes compilations of significant scientific and technical data and information deemed to be of continuing reference value. NASA's counterpart of peer-reviewed formal professional papers but has less stringent limitations on manuscript length and extent of graphic presentations.

- TECHNICAL MEMORANDUM. Scientific and technical findings that are preliminary or of specialized interest, e.g., quick release reports, working papers, and bibliographies that contain minimal annotation. Does not contain extensive analysis.

- CONTRACTOR REPORT. Scientific and technical findings by NASA-sponsored contractors and grantees.

- CONFERENCE PUBLICATION. Collected papers from scientific and technical conferences, symposia, seminars, or other meetings sponsored or cosponsored by NASA.

- SPECIAL PUBLICATION. Scientific, technical, or historical information from NASA programs, projects, and missions, often concerned with subjects having substantial public interest.

- TECHNICAL TRANSLATION. English-language translations of foreign scientific and technical material pertinent to NASA's mission.

Specialized services that complement the STI Program Office's diverse offerings include creating custom thesauri, building customized databases, organizing and publishing research results . . . even providing videos.

For more information about the NASA STI Program Office, see the following:

- Access the NASA STI Program Home Page at ***http://www.sti.nasa.gov***

- E-mail your question via the Internet to help@sti.nasa.gov

- Fax your question to the NASA Access Help Desk at 301–621–0134

- Telephone the NASA Access Help Desk at 301–621–0390

- Write to:
  NASA Access Help Desk
  NASA Center for AeroSpace Information
  7121 Standard Drive
  Hanover, MD 21076

NASA/TM—2005-213599

A Study of Cavitation-Ignition Bubble Combustion

Quang-Viet Nguyen and David A. Jacqmin
Glenn Research Center, Cleveland, Ohio

National Aeronautics and
Space Administration

Glenn Research Center

August 2005

Acknowledgments

This work was supported by the U.S. Department of Energy under a partially-reimbursable Space Act Agreement SAA–3–547 (Department of Energy Interagency Agreement number DE–A105–02OR22929), and in part, by the Strategic Research Fund (SRF) at NASA Glenn Research Center. The authors thank Gregg Calhoun, QSS Group, Inc., for the facilities operations engineering services, gas analysis, and trouble-shooting; John Zilka, University of Toledo, for his assistance in conducting the experiments; Ray Lotenero and James Sexton, Akima Corporation, for building the flow reactor apparatus; Rod Berriker, ZIN Technologies, for the flow systems design; Jackie Corrigan, University of Dayton, for help with the parametric studies using the computer model; Martin Rabinowitz and James Conklin, ORNL, for helpful discussions; and Paul Penko for his suggestions in the preparation of the manuscript.

Available from

NASA Center for Aerospace Information
7121 Standard Drive
Hanover, MD 21076

National Technical Information Service
5285 Port Royal Road
Springfield, VA 22100

Available electronically at http://gltrs.grc.nasa.gov

A Study of Cavitation-Ignition Bubble Combustion

Quang-Viet Nguyen and David A. Jacqmin
National Aeronautics and Space Administration
Glenn Research Center
Cleveland, Ohio 44135

Abstract

We present the results of an experimental and computational study of the physics and chemistry of cavitation-ignition bubble combustion (CIBC), a process that occurs when combustible gaseous mixtures are ignited by the high temperatures found inside a rapidly collapsing bubble. The CIBC process is similar to that in a diesel engine. However, the length scales are very small (μm to nm) and the time scales are very brief (μs to fs). Furthermore, the process takes place inside a micro-spherical chamber with variable dimensions rather than in a macro-cylindrical metal chamber with fixed dimensions. We computationally model the CIBC process using a 1- and 0-dimensional time-dependent compressible fluid-dynamics code that includes finite-rate chemistry. The computational model of the CIBC process indicates that gas-phase reactions within the bubble occur and produce CO and other by-products of combustion, heat and mechanical energy release through a bubble volume-expansion phase. The model shows that the CIBC process is sensitive to the fuel-air mixture ratio, the initial bubble diameter, and the acoustic pressure forcing amplitude. We experimentally demonstrate the CIBC process using an ultrasonically excited cavitation flow reactor. In the flow reactor, we subject gaseous mixtures of C_3H_8-air and CH_4-air bubbles in liquid water, and methanol vapor-air bubbles in liquid methanol, to circa 100 W of acoustic power at a frequency of 20 kHz. We measure small amounts (up to 160 ppm) of carbon monoxide (CO) emitted as a byproduct of the gas-phase chemical reactions or combustion within the collapsing bubbles. We find that the CO production is proportional to the acoustic power level delivered to the CIBC flow reactor. The results of the model were found to be consistent with the measured experimental results. Based on the experimental data, and supported by the results of the computational model and previous reports of the "micro-diesel effect" in industrial hydraulic systems, we determined that gas-phase chemical reactions that are initiated by the high temperatures within a collapsing bubble are indeed possible and exist in ultrasonically- and hydrodynamically-induced cavitation. Using the results from the computer model of CIBC of a CH_4-air bubble in water, we find that, in theory, it may be possible to develop a hydraulic-CIBC engine that produces net power. The results of the model indicate that such an engine would require at minimum the following conditions to operate at a break-even point: a liquid flow rate of about 114 liter $\cdot$ min^{-1} (31 gal $\cdot$ min^{-1}) with a 10 percent bubble void fraction of approximately 10 μm diameter CH_4-air bubbles in water, with an equivalence ratio of about 1.25, and a pressure drop of about 21 kPa (3 psid) provided by a venturi with a pressure recovery factor of at least 85 percent. A significant result of this finding is that a hydraulic-CIBC engine requires a venturi or other pressure recovering device to operate in a self-sustaining mode.

Introduction

In recent years sonoluminescence (SL), the production of light from sound resulting from the cavitational collapse of a bubble, has been an active and intense area of study because of the uniquely high temperatures and pressures obtainable using SL. Useful reviews of this phenomenon have been written by Barber (1997) and Brenner et al. (2000). This report deals with a related but new field of research called cavitation-ignition bubble combustion (CIBC), or the ignition and subsequent burning of a gaseous mixture inside a fuel-air bubble caused by adiabatic compression heating that results from

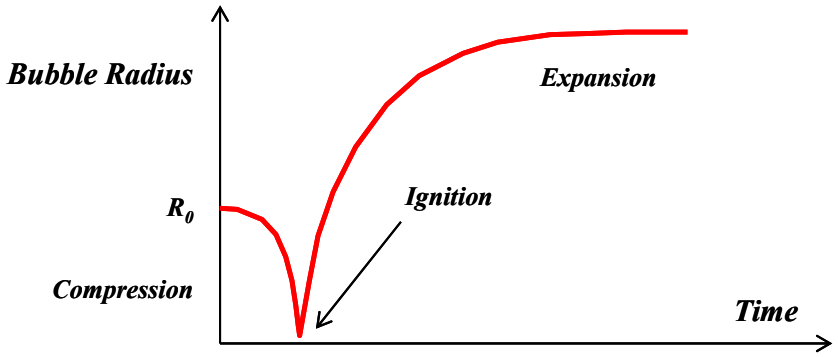

Figure 1.—Graphical depiction of the cavitation-ignition bubble combustion (CIBC) process. After an initial expansion phase resulting from cavitation, a bubble collapses rapidly due to high inertial forces that act on the bubble wall; the collapse is so sudden that an adiabatic compression heating of the contents occurs. This heating ignites the contents much like a diesel engine. In fact, this process has long been known to cause degradation of hydraulic oils and is termed the "micro-diesel" effect. The heat release and change in product moles resulting from combustion causes the bubble radius to grow to a larger radius than before, thereby producing volumetric expansion work.

cavitational collapse as depicted in figure 1. The occurrence of combustion in a fuel-air mixture inside a hydraulic-cavitation-induced collapsing bubble has been identified and known for quite some time (Lohrentz, 1968). However, it has always been considered a problem and many studies have been aimed at eliminating it as an undesirable occurrence in hydraulic fluid systems. Here however, we look at CIBC as a possible means of generating mechanical power in a way similar to a diesel engine. Furthermore, we do not limit our study to hydraulic cavitation but also consider sound-induced cavitation (sonocavitation).

There have been many previous studies of effects in or caused by cavitation. In many of these studies, cavitation has long been regarded as a problem in hydraulic systems as it causes the mechanical degradation of hydraulic components such as valves and orifices (Hobbs and McCloy, 1972). Additionally, cavitation can be responsible for the chemical degradation of the working hydraulic fluid (Totten et al., 1998; Koivula and Ellman, 1998). In particular, it has long been known that the entrainment of air into hydrocarbon-based hydraulic fluids (oils), causes a rapid degradation in the fluid properties (Staeck, 1987) from the so-called "micro-diesel" effect (Backe and Lipphardht, 1976; Svedberg et al., 1999) in which the cavitational collapse of the oil heats air inside the bubbles to the point of oxidizing or burning the oil vapor. The early investigations of Lohrentz (1968) followed by the experiments of Backe and Lipphardt (1976) showed that flashes of light resulting from the combustion of the oil vapor and air, are emitted from these bubbles as they collapse. Various techniques have been advanced to separate air bubbles from hydraulic oils to minimize this degradation and to reduce the oil temperature (see for example, Suzuki et al. 1997).

Separate from the above studies of cavitation and its effect on the properties of the working hydraulic fluid are studies of bubble combustion in the context of two-phase flow reactors in which bubbles provide the interface and surface area for gas-liquid reactions. In these studies, cavitation is not used for ignition but the contents of the gaseous bubble are ignited and reaction takes place through bulk heating. Studies include the theory of bubble displacement reactors (Likachev et al., 1991), bubble-column reactors (Carbonell and Guirardello, 1997), studies of oscillating combustible gas bubbles (Gol'dshtein et al., 1998), and premixed combustion by blowing air bubbles into liquid fuels (Kitano and Shiba, 1996).

Cavitation to purposefully effect chemical and morphological changes was pioneered by Suslick who showed that sonocavitation could be used to produce new nano-particles, synthesize new compounds, and even process bio-medical materials (Suslick et al., 1999). Hydrodynamic cavitation has also been experimentally shown to effect chemical reactions (Suslick et al., 1997; Pandit et al., 1999) in aqueous compounds. More recently, efforts have been made by several groups to model both the hydrodynamics and chemistry of cavitating flows (Gong and Hart, 1998 and 1999; Colussi et al., 1998). These studies indicate that the rapid heating and cooling of cavitational collapse provides several benefits not found using other chemical processing techniques, the most notable of which is the extremely rapid cooling rate of 10^{10} K sec^{-1} (Suslick et al., 1999) that enables the "freezing" of certain compounds after they are generated under the high and intense pressures encountered within the collapsing bubbles. Other effects such as mixture segregation from differential mass transport within collapsing bubbles (Storey and Szeri, 1999) and the role of shock waves inside collapsing bubbles (Vuong et al., 1999) have also been addressed. However, there is still debate as to the importance of bubble non-uniformity in affecting chemical interactions and the overall cavitation process.

Approach

Bubble cavitation can be initiated by any number of means including acoustic waves (sonocavitation), hydraulic pressure drops (hydraulic-cavitation), and laser-induced plasmas. For this report, the emphasis was principally centered on acoustically generated cavitation as this has been shown to produce the most intense temperatures and pressures in collapsing bubbles. We generated multi-bubble mixtures of premixed fuel/oxidizer in a small chamber containing (1) liquid water, or (2) a single-component liquid hydrocarbon fuel (such as methanol) that were acoustically forced to produce cavitation. The liquid water was seeded with a stream of premixed hydrocarbon fuel and oxidizer bubbles consisting of propane-air or methane-air. In the case of liquid methanol, the flow was seeded with air bubbles. The gas bubble seeds were then subjected to a high intensity acoustic field generated with a 200 W (max) acoustic driver/horn submerged in the liquid chamber. The horn produces intense localized pressure fields in excess of several atmospheres to drive the cavitation. Some of the collapsing bubbles (depending on how well the acoustic power couples into the bubble as a resonator) heat up to a high temperature sufficient to ignite the bubble contents.

To study this process, we applied a suite of diagnostics including the measurement of light emission resulting from chemical reactions, acoustic signatures, and time-averaged bulk gaseous emissions. However, we concentrated our measurements on the continuous gaseous emissions measurements of carbon dioxide (CO_2), oxides of nitrogen (NO_X) which include NO and NO_2, and carbon monoxide (CO) given off by the combusting bubble, as these are the main indicators of chemical reactions resulting from combustion. Tests conducted in liquid water, however, have the problem of gas solubility, as both CO_2 and NO_X are highly soluble in water. Thus, the major gaseous emissions were expected to be CO as it is much less soluble in water.

In parallel, we theoretically modeled the bubble-collapse event using the Gilmore equation describing the 1-dimensional (1-D) time-dependent collapse of a single bubble. A design-of-experiments approach was used for modeling and was aimed at determining the optimal conditions for cavitation-driven chemical reactions. The internal flow of the bubble was assumed to be a 1-D, time-dependent problem involving nano-scales of both length and time, and was not modeled in detail. Instead, the assumption of uniform properties within the bubble was used to simplify the modeling efforts.

The objectives of this study were as follows:

a.) Determine whether or not sonocavitation can be used to ignite mixtures of gaseous hydrocarbon fuels and oxidizers inside a bubble to release heat as evidenced by measurements of combustion by-products, heat-release, light emission, and/or other means of energy production.

b.) Develop a computational model of the CIBC process using fundamental principles of fluid dynamics, physics and chemistry. Perform an analysis of the CIBC process using the model to determine critical parameters for CIBC.
c.) From the experimental data and model, perform a final determination of the possibility or existence of CIBC.

Theory

We modeled the time-dependent behavior of the collapsing bubble with the assumption of radial symmetry to simplify the governing equations (Storey and Szeri, 1998). The flow in the cavitating bubble is then governed by the compressible Navier-Stokes equations for radial momentum, the continuity equation and the energy equation. The continuity equation is given by:

$$\frac{\partial \rho}{\partial t} + \frac{1}{r^2}\frac{\partial}{\partial r}\left(r^2 \rho \upsilon\right) = 0\,, \tag{1}$$

where r is the radial direction, t is time, ρ is the gas density and υ is the radial velocity. The momentum equation is given by:

$$\frac{\partial \rho \upsilon}{\partial t} + \frac{1}{r^2}\frac{\partial}{\partial r}\left(r^2 \rho \upsilon^2\right) = -\frac{\partial p}{\partial r} - \frac{1}{r^2}\frac{\partial}{\partial r}\left(r^2 \tau_{rr}\right) + \frac{\tau_{\theta\theta} + \tau_{\phi\phi}}{r}\,, \tag{2}$$

where p is the pressure. The τ terms represent the normal stresses in the fluid. Because of radial symmetry, these reduce to

$$\tau_{\theta\theta} = \tau_{\phi\phi} = -\frac{1}{2}\tau_{rr} = \frac{2}{3}\mu\left(\frac{\partial \upsilon}{\partial r} - \frac{\upsilon}{r}\right). \tag{3}$$

The viscosity μ is in general a function of temperature and composition. The evolution equation for the temperature T is given by:

$$\rho C_\upsilon \frac{DT}{Dt} = -\frac{1}{r^2}\frac{\partial r^2 q}{\partial r} - T\left(\frac{\partial p}{\partial T}\right)_\rho \frac{1}{r^2}\frac{\partial r^2 \upsilon}{\partial r} - \tau_{rr}\frac{\partial \upsilon}{\partial r} - \upsilon\frac{\tau_{\theta\theta} + \tau_{\phi\phi}}{r} + Q_C\,. \tag{4}$$

Here, the term DT/Dt is the material derivative given by $\partial/\partial t + \upsilon\partial/\partial r$. The term Q_C is the heat per unit volume that is generated due to chemical reactions. The term q is the heat transfer due to conduction, and is given by:

$$q = -k\frac{\partial T}{\partial r}\,, \tag{5}$$

where k is the thermal conductivity. The term C_υ is the specific heat at constant volume per unit mass of bubble gas. Hence, k and C_υ may both be a function of temperature, bubble gas composition and pressure.

The conservation equations for the chemical species are

$$\frac{\partial \rho_i}{\partial t} + \frac{1}{r^2}\frac{\partial}{\partial r}\left(r^2 \rho_i \upsilon\right) = M_i\,, \tag{6}$$

where M_i is the rate of change in the density of the chemical species i from chemical reactions. Diffusion currents are neglected in the calculations. The chemical heat release term, Q_C, is given in terms of the M_i by

$$Q_C = \sum_i M_i U_i \,, \tag{7}$$

where U_i is the internal energy per unit mass of material i.

The radius of the bubble changes through the mechanical interactions between its gaseous contents and liquid surroundings. The flow in the liquid is nearly incompressible and can be expressed by the Gilmore equation (Brenner et al., 2002). This is:

$$R(1-R_t/c)\,R_{tt} + \frac{3}{2}(1-R_t/3c)R_t^2 = (1+R_t/c)\,H_d + \frac{1}{c}(1-R_t/c)\,R\frac{dH_d}{dt}\,, \tag{8}$$

where R is the radius of the bubble, c the sound speed at the bubble wall, and H_d the liquid enthalpy at the bubble wall minus the enthalpy at infinity. The t subscripts indicate time derivatives. We use a liquid equation of state of the modified Tait form (Prosperetti and Lezzi, 1986)

$$\frac{P+B}{P_0+B} = \left(\frac{\rho}{\rho_0}\right)^n, \tag{9}$$

where B = 3049.13 bar and n = 7.15 gives an excellent fit for water vapor up to 10^5 bar. The enthalpy difference between the bubble wall and the far-field can then be written as

$$H_d = \frac{n}{n-1}\left(\frac{P_B+B}{\rho_B} - \frac{P_\infty+B}{\rho_\infty}\right) \tag{10}$$

and

$$\frac{dH_d}{dt} = \frac{1}{\rho_B}\frac{dP_B}{dt} - \frac{1}{\rho_\infty}\frac{dP_\infty}{dt}\,. \tag{11}$$

The B subscript indicates liquid quantities at the bubble wall. P_∞ is the far-field acoustic pressure, and is what forces the bubble motion.

Multi-Shell Numerical Model

Prior to our adoption of the assumption of uniform internal bubble flow properties, we performed a series of computational tests using a multi-shell model to incorporate the effects of internal-flow spatial non-uniformity. The multi-shell model divided the internal flow-field into a series (up to 20) of concentric shells with heat, mass, and momentum transfer. To keep the chemical kinetics simple, the effects of combustion were tested in the multi-shell model using some very simple chemical reaction models: 1) instantaneous chemical conversion and heat release where the gas temperature exceeds a given temperature; 2) heat release and chemical conversion that depends exponentially on temperature and linearly on the remaining amount of combustible material. The first model was chosen to maximize the likelihood of shock formation. We found that this occurred only under extreme conditions. In most situations, conditions within the bubble stayed fairly smooth. This was especially true for pressure, and mostly true for temperature, even near the bubble wall. This finding of little formation of spatial structure

is consistent with the review of Brenner et al., (2002) that show sonoluminescing bubbles are usually shock-free, though sometimes can be generated (Yuan et al., 1998)

We concluded that a single-shell (or homogeneous properties) model is adequate for further computational investigations of CIBC. The single-shell model has the advantage of fast computation and therefore offers the opportunity to fully compute complex chemical mechanisms.

Single-Shell Numerical Model

The single-shell model is equivalent to approximating the conditions within the cavitating bubble as uniform. The mass M in the bubble is constant, as evaporation effects are neglected. The amount of each chemical species and the total number of moles of gaseous chemical species vary as a function of time from the effects of chemical reactions (combustion). The chemistry was calculated using the CHEMKIN subroutine package (Kee et al., 1989) in conjunction with a methane-air chemical kinetic mechanism (Bowman et al.). As with the continuum model, the changes in the radius and volume of the bubble are determined by the Gilmore equation.

The perfect gas law is assumed,

$$P = NR_g T / V \,, \tag{12}$$

where N is the time-varying number of moles, V is the bubble volume, and R_g is the universal gas constant. The temperature of the gas varies with the internal energy according to

$$\frac{dT}{dt} = \frac{1}{Mc_{\upsilon m}}\left(\frac{dU}{dt} + Q_C\right) = \frac{1}{Nc_{\upsilon n}}\left(\frac{dU}{dt} + Q_C\right), \tag{13}$$

where $c_{\upsilon m}$ is the constant-volume specific heat per mixture unit mass and $c_{\upsilon m}$ is the constant-volume specific heat of mixture per unit mole. These are functions of temperature and bubble composition as calculated by the CHEMKIN subroutine package (Kee et al., 1989). The time variation of U is given by

$$\frac{dU}{dt} = Q_k - \frac{NR_g T}{V}\frac{dV}{dt} \,, \tag{14}$$

where Q_C is the chemical heat release, and Q_k is the amount of heat conducted into the bubble is given by

$$Q_k = \alpha k\left(T_{LIQ} - T_{GAS}\right)/ A \ \,, \tag{15}$$

Where α is a proportionality constant (adjustment factor) and A is the bubble wall area. Results were found to be insensitive to the value of α (Brenner et al., 2002). This is because the bubble-collapse period, which is the period of greatest interest, is so fast that it is essentially adiabatic. The conductivity k was simplified to a constant, chosen to be typical of the gases at the given liquid temperature. This is the temperature range where the bubble exists most of the time.

With regards to the numerical time-steps chosen for the simulations: all calculations were explicit, chemical reactions therefore required short-time steps at high temperatures. This apparent inefficiency is acceptable because at high temperatures the bubble radius evolution proceeds extremely rapidly, which, to capture this change, also requires small time-steps in the picosecond to femtosecond range. The time-step size was calculated at each time-step using simple formulas involving the powers of bubble radius and temperature. The formulations for calculating the variable time-steps turned out well: when we included the full chemical kinetic mechanism with 279 elementary reaction-steps, it was still possible to calculate hundreds of thousands of bubble radius time-steps per CPU second. As a result, the

computational time for a few bubble oscillations is typically on the order of several minutes to an hour on a standard desktop workstation.

Experimental Apparatus

We used an acoustically excited sonocavitation flow reactor setup to demonstrate the existence of CIBC. The experimental apparatus is given schematically in figure 2. This shows the recirculating liquid flow system which provides the bulk flow of the working fluid, the gaseous flow system which provides a controllable mixture of gaseous reactants, the gaseous emissions analyzer, and an automated facility data acquisition and control system.

At the center of the system is an optically accessible flow reactor that is constructed using standard stainless steel vacuum hardware with fused-silica windows on 3 sides of the two 6-way crosses. The working liquid (distilled water or spectroscopic grade methanol) enters from the bottom of the reactor where a gaseous mixture of fuel and oxidizer is introduced into the liquid using a sintered stainless steel filter element (7 μm). The resulting two-phase flow of liquid and bubbles is then introduced to the upper section of the flow reactor through a 2 mm diameter orifice located at the center of a 20 mm diameter disk made of titanium. This is referred to as the "anvil" after a configuration used by Hobbs et al. (1969) and Hobbs and Rachman (1970). The two-phase flow issuing from the orifice forms a jet that impinges on the face of a 12.7 mm diameter titanium ultrasonic transducer horn that is spaced between 2 to 10 mm from the anvil. Titanium is used for wear resistance as it has one of the lowest cavitational erosion rates of any metal (Hobbs and McCloy, 1972). Figure 3 shows a photograph of the hammer and anvil configura-tion with the acoustic horn in the off state. Figure 3 shows a toroid-like collection of bubbles trapped in

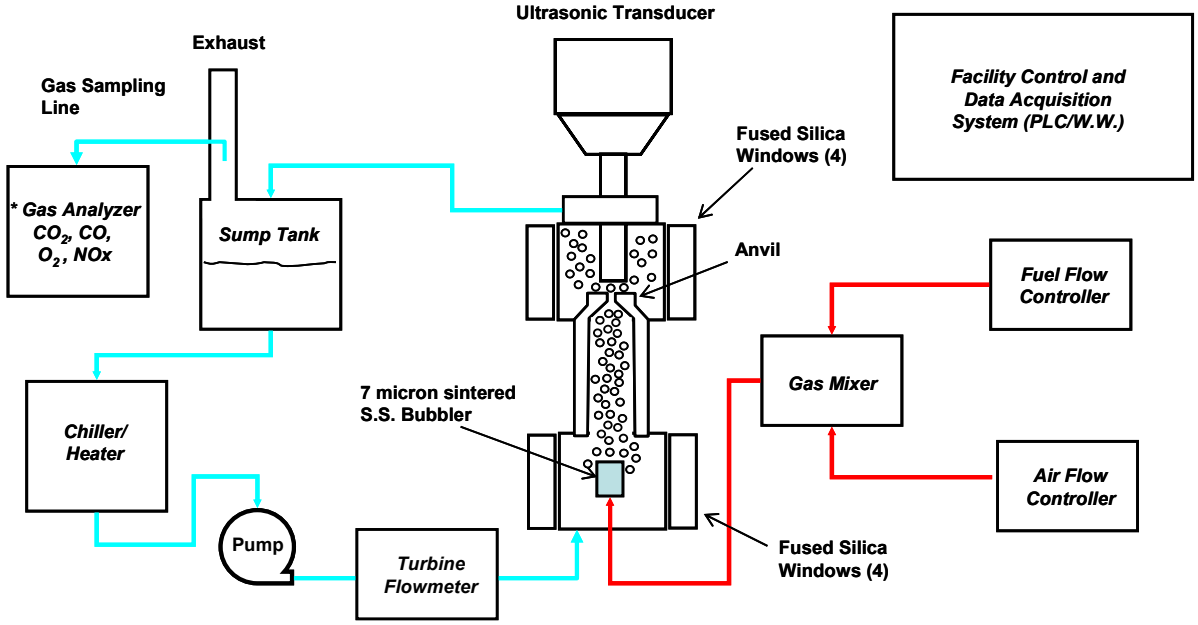

Figure 2.—Schematic of the sonocavitation flow reactor system. There are two separate flow systems: recirculating liquid and gaseous reactants. The recirculating liquid flow system uses a gear pump to drive the bulk liquid through the flow reactor. The gaseous flow control system meters and mixes the fuel/oxidizer mixture before delivering it into the reactor using a sintered filter bubbler. The two-phase mixture then impinges onto an ultrasonic transducer horn in a "hammer and anvil" geometry. The gaseous emissions that result from the CIBC process are then separated in the sump and are analyzed. All aspects of the apparatus are controlled and recorded from a programmable logic controller (PLC) in conjunction with software and a PC.

the recirculating flow field set up by the stagnation point flow resulting from the impingement of the jet on the face of the acoustic transducer horn. We chose this type of flow geometry because: (1) it provides an intense and uniform acoustic pressure field that all portions of the flow must pass through; (2) it also provides excellent optical access to view the process from the outside; (3) the residence time that the fluids are in contact with the high intensity sound field can be varied by adjusting the gap between the hammer and anvil or the bulk flow rate of the fluid; and (4) the stagnation point flow geometry is well-understood and provides clear boundary conditions that are useful from a computational-fluid dynamics (CFD) modeling standpoint.

After the two-phase flow of liquid and bubbles undergoes acoustically induced cavitation, and in some cases, cavitation-ignition bubble combustion, the flow and its resulting gaseous combustion byproducts are then deposited into a stainless steel sump tank (8 liter capacity, typically filled to 4 liters) to permit the liquid and gases to settle and separate. The gaseous emissions that are separated from the liquid exit through a vent tube directed to an exhaust ventilation hood. A small gaseous-sampling probe inside the vent tube extracts a portion of the vented gases. This is then dried using an anhydrous calcium sulfate desiccant pack, then drawn into a gas analyzer for the determination of oxygen (O_2), carbon dioxide (CO_2), carbon monoxide (CO), oxides of nitrogen (NO_X), and hydrocarbons (HC) or sulfur dioxide (SO_2). The gas analyzer (Horiba, PG-250) uses non-dispersive infrared (NDIR) techniques to measure the CO, CO_2 and HC/SO_2 concentrations, chemiluminescence to measure the NO_X concentration, and an electro-galvanic cell to measure the O_2 concentration. All gases are calibrated using NIST traceable calibration gas standards. The liquid flow in the sump is then recirculated through the system after going through a temperature controlled heat exchanger that stabilizes the temperature of the liquid (20-22 C). A filter (10 μm) then removes larger particulates resulting from the cavitational erosion. A magnetically-coupled ceramic gear pump (up to 1.5 liter · min^{-1}) provides the positive pressure to drive the fluid through the system. A turbine flow meter measures the fluid flow rate. Throughout the flow path, the temperatures and pressures of the bulk fluid at critical points are monitored and recorded using type-K

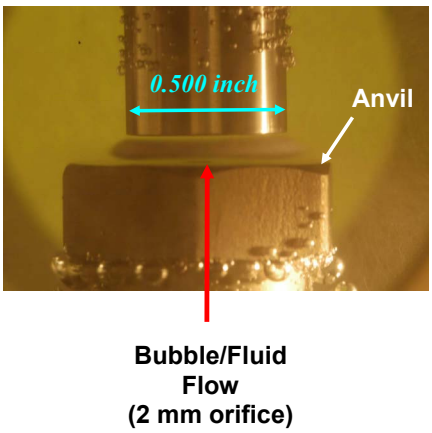

Figure 3.—Photograph of the hammer and anvil flow reactor geometry. The two-phase flow enters from the bottom through a 2 mm diameter orifice and impinges on the 12.7 mm (0.50 inch) diameter ultrasonic transducer horn. Both the ultrasonic transducer horn (the hammer) and the anvil are made of titanium for cavitational erosion resistance. In this photograph, the ultrasonic transducer is turned off, but the liquid flow is turned on. The stagnation point flow produces a small recirculation zone that traps bubbles in a toroidal pattern above the anvil.

thermocouples and high precision electronic pressure transducers (0.5 kPa accuracy). The flow leaving the turbine flow meter is then directed to the bottom of the flow reactor where the premixed gases are injected as bubbles.

The gases are provided from pressure regulated cylinders and metered and controlled using precision thermal conductivity mass flow controllers with a specified 2 percent accuracy over the flow range (350 sccm max). The flow meters are calibrated using an electronic soap-bubble type volumetric flow calibrator. The gases used are dry air, argon (Ar), nitrogen (N_2), propane (C_3H_8), and methane (CH_4). The metered gas flows from the fuel and oxidizer side of the flow systems are then mixed using a custom co-annular tube mixer. In this type of flow mixer the fuel flows down the inner central tube, while the oxidizer is fed in through the annular space. The oxidizer is injected through radially directed holes along the inner tube wall and mixed with the fuel. In this way, a fully premixed gas flow is established quickly and efficiently through the resulting high-shear mixing action of the oxidizer jets upon the central core flow. The gases exiting the mixer then pass through a check valve, and finally to the sintered filter element that serves as the gas bubbler. All gas flow pressures, temperatures and flow rates are measured and recorded with 16-bit precision at a rate of 10 Hz using the automated data acquisition and control system. Typical gas flow rates range from 10 to 100 sccm for the fuel and 100 to 300 sccm for the air. Typical liquid flow rates ranged from 1.0 to 1.5 liter $\cdot$ min^{-1}(1 $cm^3 \cdot min^{-1}$ accuracy).

The automated data acquisition and control system uses a programmable logic controller (PLC) system with various analog and digital input/output interfaces. The PLC, in conjunction with custom developed software and two rack-mounted PC's, control all aspects of the apparatus including safety related interlocks and shutdown processes, remote valve actuation, pump speed, gas flow rate control, the ultrasonic power setting, all measured instrumentation data such as pressures and temperatures, and gaseous emissions analyzer readings. Figure 4 shows a photograph of the apparatus and the laboratory that was dedicated to this study. In figure 4, the PLC instrumentation rack is in the background along with the computer monitors used to control the software. The gas analyzer is on the left, the power supply and driver for the ultrasonic system is behind the computer monitor in the foreground, and a stereo-microscope in the foreground is focused on the optically accessible hammer and anvil flow reactor. Figure 5 shows a closer view of the flow reactor setup where the optical access windows for the flow reactor can be seen; at the top of the flow reactor is the ultrasonic transducer mounted in a vertical position.

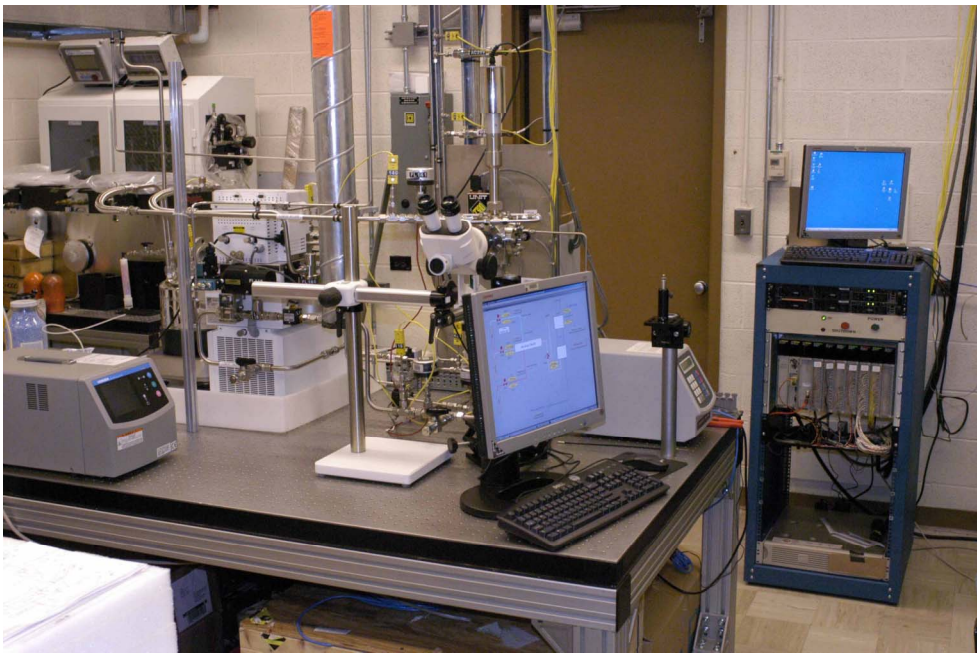

Figure 4.—Photograph of the CIBC flow reactor system and laboratory.

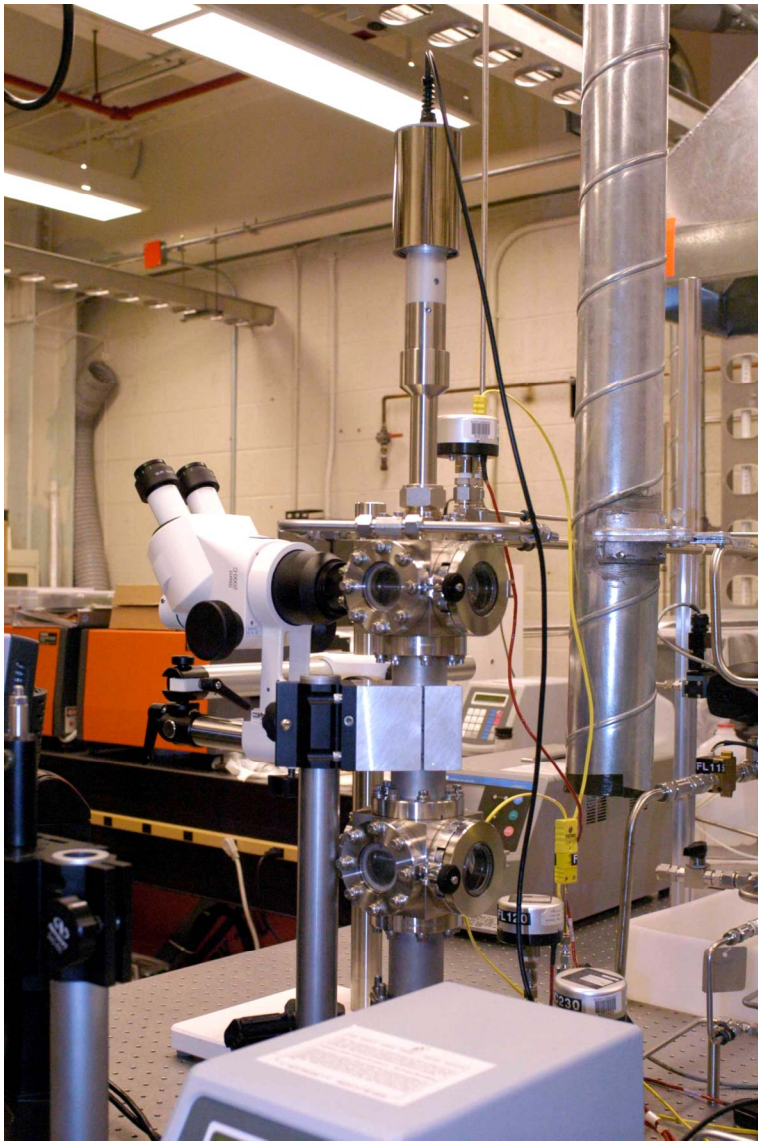

Figure 5.—Photograph (detail) of the optically accessible flow reactor system.

Results of Computer Model of CIBC Process

We begin with a discussion of the results of the computational model of cavitation-ignition bubble combustion. We chose to model the process for a gaseous bubble in liquid water. The working fluid used in many hydraulic devices is similar to automatic transmission fluid (ATF). However, ATF is a widely varying complex mixture of mineral oils and many chemical additives designed to stabilize the oil, prevent oxidation, enhance lubricity, etc., and these additives complicate the interpretation of experimental results. Thus, for the purposes of demonstrating CIBC, we chose two single component liquids: water and methanol. Water has other advantages such as being clean and easy to work with, has a

high surface tension force, and is relatively inert from a combustion standpoint. We used methanol (CH_3OH) as a hydrocarbon based working fluid because it too, is relatively clean and easy too work with.

The acoustic or sonocavitation pressure wave that is used to drive the CIBC process is modeled as a far-field sine wave at 20 kHz, with an amplitude up to 1.2 atm. We further assume that the bubble rest radius is initially 4.5 μm (baseline case). The 4.5 μm radius is used as the baseline case so that the non-combustion results of the simulations can be compared with other studies (Storey and Szeri, 1999). Comparisons of the results of our baseline simulation (no chemistry) with these other studies showed excellent agreement. In order to model the chemical kinetics properly, we use methane-air as the reactant gases inside the bubble as there are well characterized and validated chemical kinetic mechanisms for methane-air chemistry (Bowman et al.). Basically, we are trying to remove as many unknowns and ambiguities in the problem as possible in order to distill the computational problem to a case in which the properties of both the liquid phase and gas phase are well known, or readily calculated or estimated.

Effect of Pressure Amplitude on Peak Temperature

Figure 6 shows the results of the CIBC simulation for a methane-air bubble with a stoichiometric equivalence ratio ($\phi = 1.0$) and a 1.110 atm pressure amplitude forcing at 20 kHz for a 4.5 μm radius bubble in 350 K water. The upper plot shows the bubble radius and temperature as a function of time (out to 150 microseconds). In this plot we can see that the bubble oscillations are steady and repeatable from cycle to cycle. We can also see that there is the characteristic bubble "bounce" that decays within 10 small oscillations at the end of the collapse due to the acoustic impedance mismatch between the bubble and the water. The lower plot shows the chemical species concentrations for two of the reactants: methane and oxygen. In figure 6 we can see that although the peak temperatures reach as high as 1800 K, there is little or no combustion as evidenced by the lack of consumption of either methane or oxygen. This is due to the short times (< 1 ns) that high temperatures persist, and this condition is insufficient to result in enough

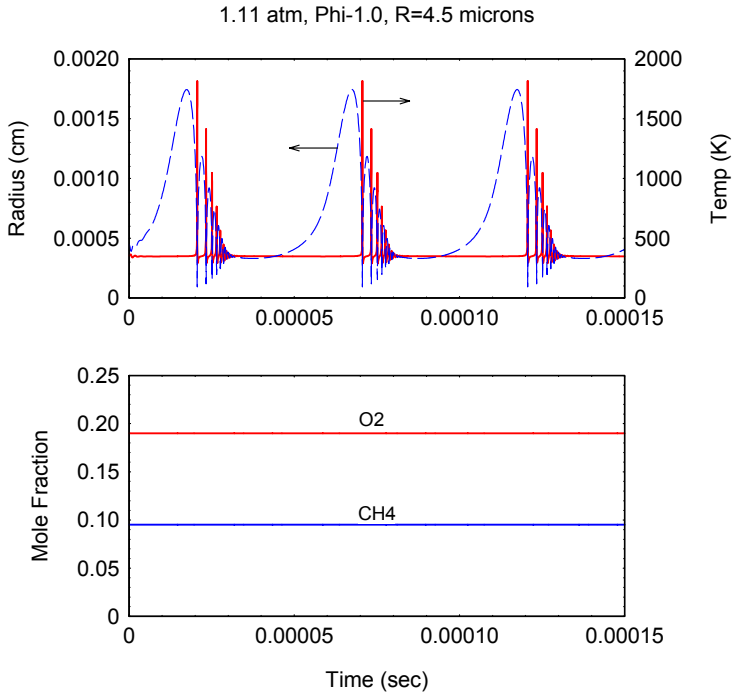

Figure 6.—Results of CIBC simulation for methane-air bubble in water where combustion does not occur (1.11 atm forcing amplitude).

molecular collisions to result in significant chain-branching chemical reactions that are required of combustion. Figure 7 shows the simulation for the same bubble, except that the pressure amplitude has been slightly raised to 1.115 atm, and at this condition, the peak temperatures are just above 2000 K. At this temperature, signs of chemical reactions are apparent as evidenced by the slight consumption of CH_4, and the production of H_2O, OH and CO at the peak temperature points. In figure 8, we now increase the pressure amplitude a little more to 1.14 atm, and we can see the resulting dramatic increase in the chemistry and what appears to be combustion resulting from the cavitational heating. From figure 8, we can also see that the peak temperatures are still continuing to rise with each major bubble collapse as more energy is released from the methane oxidation with each cycle. This can clearly be seen in the lower plot of figure 8 which shows the CH_4 concentration dropping in a step-like function with each temperature peak. Similarly, the O_2 is being consumed with each oscillation and H_2O and CO are both being generated in a step-like manner. Note that because this condition is marginally enough to produce combustion, approximately 3 major oscillation cycles are required to completely consume the CH_4. Similar step-like changes in chemical concentrations following each peak temperature spike were also reported by Gong and Hart (1998) in their simulation of a collapsing bubble with chemistry.

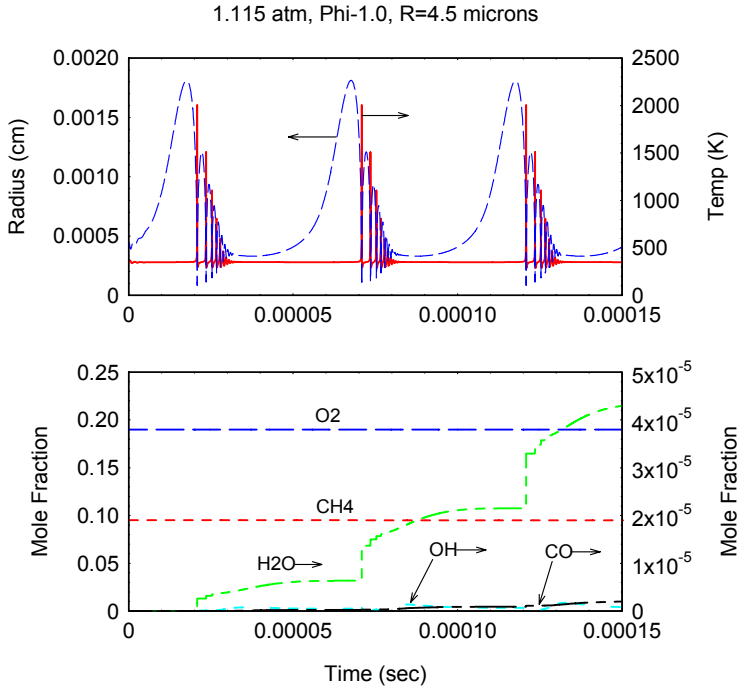

Figure 7.—Results of CIBC simulation for methane-air bubble in water where combustion caused by bubble collapse has just started to occur (1.115 atm forcing amplitude). Note the small amount of H_2O and OH being generated after each collapse.

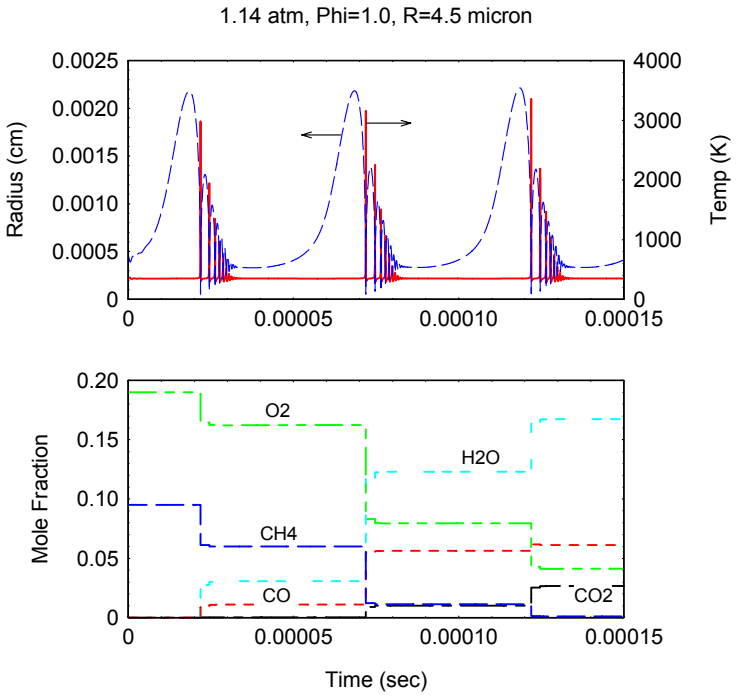

Figure 8.—Results of CIBC simulation for methane-air bubble in water where combustion is just starting to occur (1.14 atm forcing amplitude). The upper plot shows the radius and temperature of the bubble, the lower plot shows the chemical species mole fraction for the major combustion products. Note that the methane is essentially completely consumed by the third cycle.

Figure 9 shows the results of the CIBC simulation for the same bubble with a more powerful pressure amplitude of 1.19 atm. At this amplitude, the initial peak temperature is in excess of 4000 K, but notice that the subsequent peak temperatures are much lower (about 3700 K). This indicates that the majority of the heat or energy release occurred in the first collapse which had sufficient energy to oxidize all the CH_4. However, due to the rapid cooling rates within the bubble, intermediate by-products of combustion such as CO are frozen and are slowly oxidized in subsequent bubble collapse cycles. From the change in the bubble radius resulting in the heat release after combustion (highlighted by the arrows), volumetric change in the bubble may provide a way of extracting useful $\int pdV$ work. Figure 9 also highlights another aspect of CIBC: the production of nitric oxide (NO) as a result of the thermal NO_X mechanism. From the lower plot in figure 9, we can see that there is a significant amount of NO_X generated with each collapse. Note that there does not even have to be combustion to have NO_X as a plain air bubble subjected to the effects of cavitation will also produce it, as observed by (Wakeford et al., 1998).

Figure 10 summarizes the effect of the acoustic pressure amplitude on the peak bubble temperature. From figure 10, we can see that acoustic amplitudes of less than 1.00 atm really have no effect on the cavitational heating of a bubble; above 1.05 atm the bubble peak temperature starts to rise rapidly, and above 1.12 atm chemical reactions that can be described as combustion start to take place. Our simulations show that bubble combustion as evidenced by the actual chemical production of combustion by-products does not happen in stoichiometric methane-air bubbles in water until a temperature of 2000 K is reached. The behavior of the peak temperature curve does not show an abrupt change at 2000 K, as the

effect is gradual. The result shown in figure 9 indicates that the ignition of the contents of a bubble depends on the peak temperature in a subtle way, and that the temperature change due to heat release is less than the temperature rise of the bubble resulting from cavitational collapse alone. The significance of this finding is that the flows used by hydraulic-CIBC devices must undergo a significant flow restriction in order to generate the necessary pressure drop to induce hydrodynamic cavitation with a high pressure amplitude differential to produce cavitation ignition. With hydrodynamic cavitation, a significant pressure drop, if not recuperated using devices such as a venturi, will cause a significant energy loss penalty. Thus it is highly unlikely that a hydrodynamic cavitation based CIBC engine will produce net power without the implementation of some form of pressure loss recovery system.

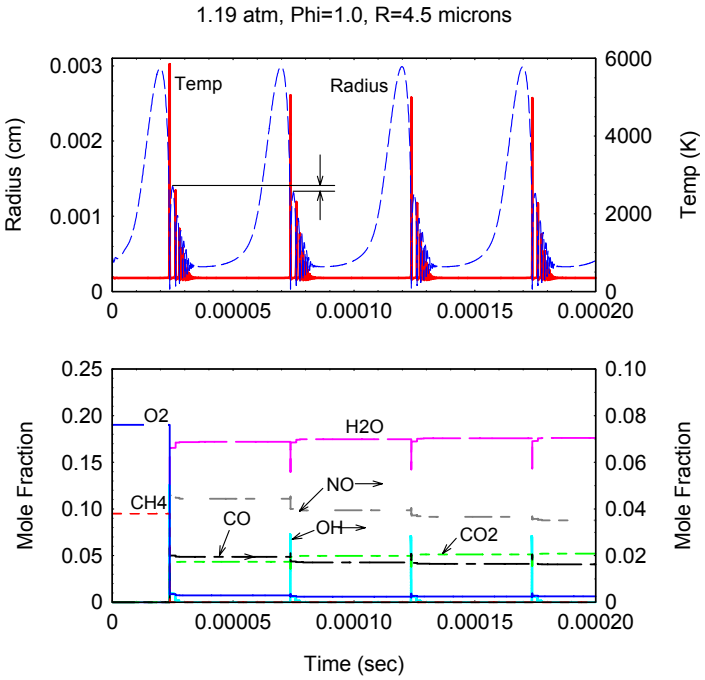

Figure 9.—Results of the computer model of CIBC with full chemistry. A stoichiometric ($\phi = 1.0$) methane-air bubble in water with an initial radius of 4.5 μm is excited with 20 kHz sound waves at an amplitude of 1.19 atm. The lower plot shows the radius and temperature as a function of time; the upper plot shows the chemical species concentrations of several key molecules. Note how the methane fuel is completely consumed after the initial collapse which then generates CO_2, H_2O, CO, OH, and NO. The subsequent collapses serve to consume the CO that was left behind from the first cycle as a result of incomplete combustion. Chemical reactions only occur when the temperature is high (where OH is visible), which corresponds to the peak of the bubble collapse.

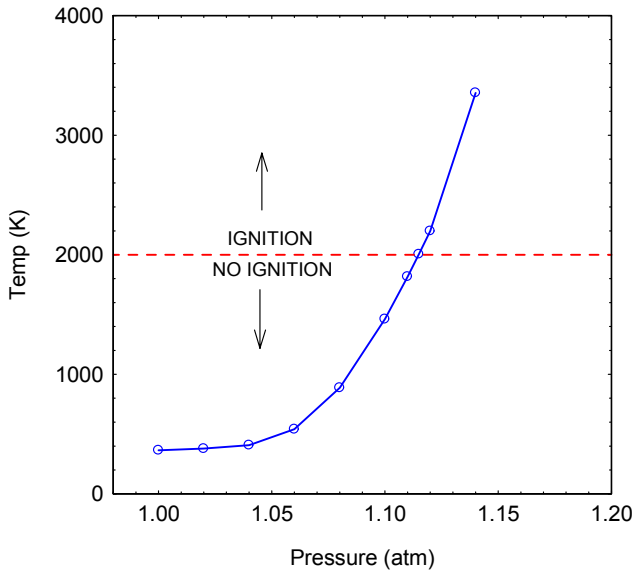

Figure 10.—Results of CIBC simulation for methane-air bubble in water showing the dependence of the temperature vs. far-field acoustic pressure. Ignition occurs at approximately 2000 K.

Figure 10 summarizes the effect of the acoustic pressure amplitude on the peak bubble temperature. From figure 10, we can see that acoustic amplitudes of less than 1.00 atm really have no effect on the cavitational heating of a bubble; above 1.05 atm the bubble peak temperature starts to rise rapidly, and above 1.12 atm chemical reactions that can be described as combustion start to take place. Our simulations show that bubble combustion as evidenced by the actual chemical production of combustion by-products does not happen in stoichiometric methane-air bubbles in water until a temperature of 2000 K is reached. The behavior of the peak temperature curve does not show an abrupt change at 2000 K, as the effect is gradual. The result shown in figure 9 indicates that the ignition of the contents of a bubble depends on the peak temperature in a subtle way, and that the temperature change due to heat release is less than the temperature rise of the bubble resulting from cavitational collapse alone. The significance of this finding is that the flows used by hydraulic-CIBC devices must undergo a significant flow restriction in order to generate the necessary pressure drop to induce hydrodynamic cavitation with a high pressure amplitude differential to produce cavitation ignition. With hydrodynamic cavitation, a significant pressure drop, if not recuperated using devices such as a venturi, will cause a significant energy loss penalty. Thus it is highly unlikely that a hydrodynamic cavitation based CIBC engine will produce net power without the implementation of some form of pressure loss recovery system.

Effect of Bubble Radius on Peak Temperatures

We now examine the effects of variations in the initial bubble radius on the peak temperature, and hence, its effect on the ignition of the bubble contents. We start with the baseline case using a stoichiometric methane-air bubble being forced at 20 kHz with a 1.19 atm pressure amplitude. Figures 11 and 12 show how the dynamic behavior of the bubble changes completely for increasingly larger bubble radii. In figure 11, the initial bubble radius is set at 20 μm, and this causes both the peak temperature and the maximum radius to vary significantly from cycle-to-cycle. Figure 12 shows the same simulation but with an initial bubble radius of 65 μm, here we can see that in addition to the peak temperatures and maximum radii being completely chaotic, the number of smaller bounce cycles is reduced and is also

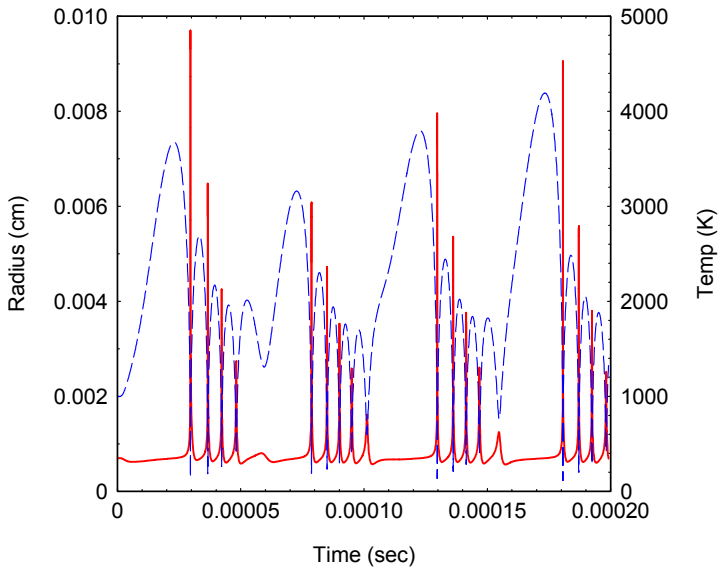

Figure 11.—Calculated variation of radius and temperature for a 20 μm initial radius methane-air bubble with $\phi = 1.0$, at 1.19 atm and 20 kHz. Note the non-uniform, almost random behavior of the bubble.

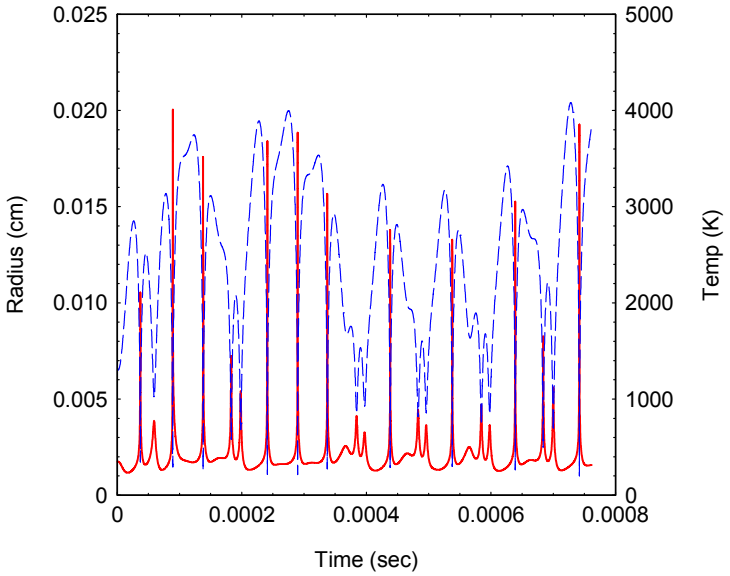

Figure 12.—Calculated variation of radius and temperature for a 65 μm initial radius methane-air bubble with $\phi = 1.0$, 1.19 atm, 20 kHz. Note the non-uniform, chaotic behavior of the bubble.

chaotic, in that sometimes there are no after bounces. These figures show that in general, the dynamics of collapsing bubbles, coupled with the chemical interactions which release heat and affect the bubble dynamics, yields a highly non-linear system (see figs. 11 and 12). If we carry out these simulations for an extended time period (10 million points) or about 1 ms of actual bubble time, and record the peak bubble temperature, we can see that the variation in the peak temperature as a function of bubble radius as shown in figure 13 is highly non-linear. Figure 13 shows that for bubble radii ranging from about 2.5 to about 150 μm, the peak bubble temperature is greater than 2000 K, which is sufficient for igniting the contents of the bubble. Figure 13 also indicates that for bubbles larger than about 20 μm in radius, multiple bubble oscillations are required to produce an ignition event (solid line). The dashed line represents the peak temperature from the first collapse, and this curve falls off significantly after about 50 μm radius. In a hydraulic-CIBC process, the cavitation collapse occurs only once for each bubble as it passes through a flow restriction device that produces the cavitation (unless the bubble is forced past multiple flow restrictions to drop the pressure repeatedly). Therefore, the lesson of this finding is that for a hydrodynamic based CIBC process it is critical to have a precise and narrow distribution of bubble sizes that are within the size range that will lead to ignition events. For sonocavitation devices, where the bubble can be subjected to repeated cycles, the sizing and distribution of the bubble radius is less critical as shown in figure 13.

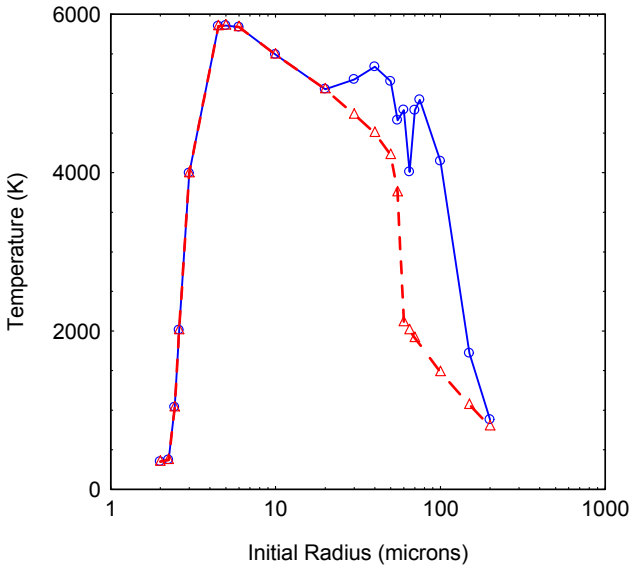

Figure 13.—Variation of maximum bubble temperature with initial bubble radius (solid line) for a $\phi = 1.0$ methane-air bubble in water with 1.19 atm forcing at 20 kHz. Note that there for bubble radii ranging from about 2.5 to 150 μm temperatures will reach above 1500 K, which should be sufficient for ignition. The maximum temperature of the first collapse is shown with the dashed line. For bubbles larger than 20 μm, more than one bubble oscillation is required to attain the maximum temperature. Thus, for the case of hydrodynamic cavitation where the bubble has only one cycle to ignite, bubbles have to be smaller than 20 μm to achieve ignition.

Work Produced by CIBC Process and Effect of Equivalence Ratio

The problem of extracting useful work or energy from the CIBC process, although it is not one of the primary questions to be answered in this study, is nonetheless important to examine from the standpoint of practical applications that could utilize CIBC. We use the computational model of CIBC to calculate the net-energy release (work output) per bubble and examine the effect of methane-air equivalence ratio to determine the optimum stoichiometry for methane-air bubbles in water. From this number we can then estimate the maximum volumetric power density of a CIBC device. As the temperature change in the bulk liquid resulting from the combustion heat-release in CIBC is negligible because of the small (1:1000) ratio of bubble density compared to liquid density, we have to assume that the energy released by a bubble resulting from CIBC must be harnessed through some other means than a net bulk temperature increase in the working fluid. As there is a change in the volume of the bubble after a CIBC event, and this change is impressed on the surrounding fluid and is sensible from a two-phase bulk fluid standpoint given enough bubbles (void fraction of say 10 percent), this volumetric change can potentially be harnessed and converted to useful work. This volumetric-change or boundary expansion work is given by:

$$W(t) = \int_{V_0}^{V(t)} p(t)dV \,, \tag{16}$$

where, $p(t)$ is the time-varying pressure and the dV is the infinitesimal change in the volume of the bubble from an initial bubble volume V_0 to the volume at time t given by $V(t)$. We define a positive value as net energy out of the bubble, and negative values as energy into the bubble (required to expand or compress the walls of the bubble for instance). We calculate $W(t)$ using a discrete summation of equation (16), and plot the results for different equivalence ratios as shown in figure 14. From figure 14, we can see that peak energy resulting from the bubble expansion (after the initial collapse and bubble oscillations) occurs

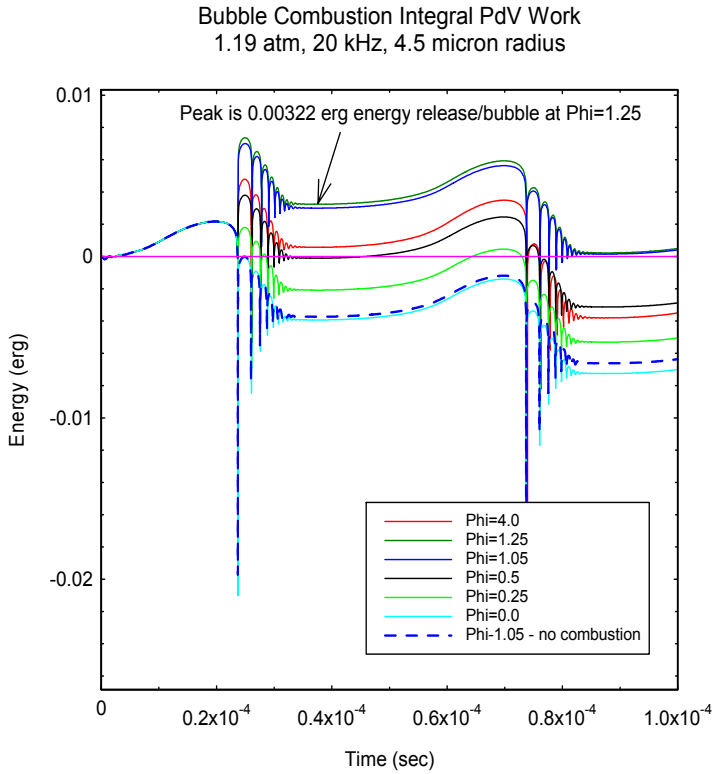

Figure 14.—Results of the computer model showing the effect of equivalence ratio on the production of $\int PdV$ work.

at about 400 microseconds. Again, the simulations assume the baseline conditions of 4.5 μm bubble radius, 20 kHz acoustic frequency, and 1.19 atm pressure amplitude for a methane-air bubble in 350 K water. We can see that for fuel-lean values, the amount of energy required to induce the cavitation (pressure forcing) is greater than energy released as a result of combustion. In fact there is a break-even point at about $\phi = 0.5$. Thus, this indicates that the CIBC process cannot produce net work for very fuel-lean fuel-air mixtures.

If we plot the maximum energy release as a function of equivalence ratio, we see that the maximum energy release produced after the bubble bounce-oscillations subsides, is 3.22×10^{-3} erg · bubble^{-1} (1 erg = 10^{7} J), and occurs at $\phi = 1.25$, as shown in figure 15. In conventional internal combustion engines, the peak energy release is typically very close to a slightly fuel-rich, but near stoichiometric ($\phi = 1.0$) point. We now calculate the number of bubbles required to produce 7.46×10^{9} erg · sec^{-1} (746 W or 1 hp) given that the maximum energy release per bubble is 3.22×10^{-3} erg · bubble^{-1}. These values, when combined, result in a value of 2.32×10^{12} bubble · sec^{-1}, which translates to a requirement of a flow rate of 53 liter · min^{-1} of gaseous flow per 746 W (1 hp) assuming uniform 4.5 μm radius bubbles. If we further assume a bubble void fraction of 10 percent, then the liquid flow rate requirement per 746 W (hp) is 530 liter · min^{-1} · hp^{-1} or 140 gal · min^{-1} · hp^{-1}.

For a pump to produce a flow with a sufficient pressure differential of 1.2 atm (121 kPa or 17.6 psid) to produce ignition-capable cavitation, the pump will require at least 783 W (1.05 hp) of power input (Lee Co., 1997) assuming that the pressure drop is obtained through a conventional flow orifice with a 27 percent pressure recovery factor (Baker, 2000). Although 783 W (1.05 hp) is only slightly higher than the 746 W (1.00 hp) input required to drive the CIBC process, we have not accounted for other losses such as friction, and inefficiencies. However, if a pressure-recovering device such as a cavitating venturi with an 85 percent pressure recovery is used (Hu et al., 1998), then the pressure drop experienced by the

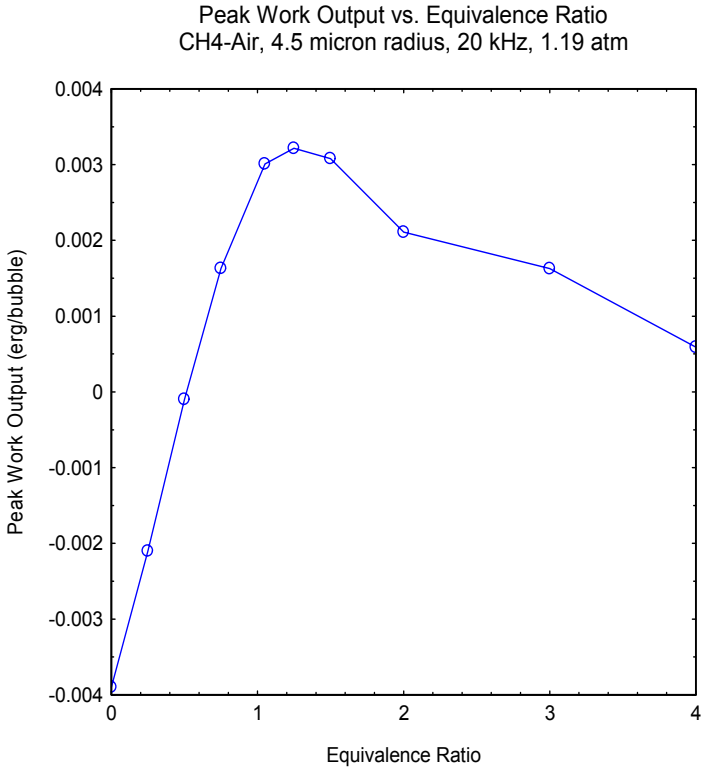

Figure 15.—Results of the computer model showing the effect of equivalence ratio on the peak energy output per bubble.

pump will be less than 21 kPa (3 psid), which translates to a pump power requirement of only 164 W (0.22 hp). Thus, if the volumetric bubble expansion power extraction from the CIBC process was perfect, a minimum liquid pump flow rate of about 114 liter · min^{-1} (31 gal · min^{-1}) with a pressure drop of about 21 kPa (3 psid) would be required for the engine to operate in a break-even or self-sustaining mode. The estimated specific volumetric flow rate from the above values is approximately 0.7 liter · min^{-1} · W^{-1}. More importantly though, this analysis reveals a very important finding: a hydraulic-CIBC engine cannot run in a self-sustaining mode unless venturi-type pressure restrictors are used to recover the excess pressure drop. The flow values above represent the minimum conditions required to develop a self-sustaining hydraulic CIBC device.

For a system operating on a hydrocarbon-based oil such as ATF, the value would be significantly different as the vapor pressure of oil based liquids is significantly lower, and this would mean that higher liquid flow rates (and higher pump input power) would be required to produce a net power output. However, the values calculated above using a methane-air bubble in water are good starting point for future estimates.

Experimental Evidence of Bubble Combustion

We performed several experiments using the previously described apparatus in an attempt to obtain data that would indicate the existence of CIBC. Perhaps the most conclusive evidence of bubble combustion would be the release of a gaseous emission consistent with the products of combustion such as CO_2, CO, or NO_X. Other indicators of combustion would include the emission of light, the generation of heat, and even the generation of a sound. However, the solubility of both CO_2 and NO_X in liquid water and methanol is high (England, 1986), and the most likely molecule for an observable gaseous emissions measurement is CO. We attempted to measure the emission of visible light (400 to 700 nm) from the CIBC process using a lens-fiber-coupled spectrograph and high sensitivity CCD camera, similar to the one used by Kojima and Nguyen (2003) for spontaneous Raman scattering studies. Although this spectrometer/CCD camera combination has single-photon sensitivity, the optical emissions in the visible spectrum were nonetheless, very faint. Thus the results were inconclusive so we do not present them here.

We noticed an intermittent but audible change in the sound that the apparatus made when the system was operated with combustion-capable gas mixtures. We then mounted a small piezoresistive pressure transducer (200 kHz bandwidth, 0.07 kPa sensitivity) to a stainless steel window blank affixed to the acoustic reaction chamber portion of the flow reactor. The transducer or microphone was mounted so that the sensor tip protruded 3 mm past the blank plate surface. The output from the microphone was then sent to an oscilloscope for storage and analysis. The sound traces showed distinct high amplitude (up to 1.5 atm) pressure peaks. The analysis of the acoustic signature data from the microphone however, proved inconclusive due to the intermittent nature of the signal and its irreproducibility. The intermittent nature of the sounds generated by the sonication process probably resulted from an inefficient coupling of the acoustic energy into the bubbles. Ideally, the bubble diameters should fall within the distribution shown in figure 13 for efficient acoustic energy transfer. We speculate that an acoustic impedance mismatch between the wavelength of the sonication waves and the bubble sizes resulted from the rather wide distribution of the bubbles. This was confirmed by our measurements of the bubble sizes discussed in the following paragraph.

The 7 μm pore bubbler element when used with distilled water produced rather large bubbles that ranged from approximately 200 μm to 2 mm in diameter (measured using microphotographs taken with a stereomicroscope and digital camera combination). This was due to two causes: small bubbles in pure water coalesce readily to form larger bubbles, and the co-flowing liquid water velocity past the bubbler pores was too slow to quickly detach the small bubbles from the surface as they were being filled by the exiting gas flow. According to the study performed by Chuang and Goldschmidt (1970) co-flowing water velocities of about 2 m · sec^{-1} are required to permit the generation of the smallest bubble sizes, whereas

the co-flow velocities in our study were much lower (0.01 m · sec^{-1}). Thus, several things can be done in future studies to improve the bubble generation process: a salt such as $MgSO_4$ can be added in small quantities to increase the short range hydration repulsion forces between two gas-liquid interfaces to prevent bubble coalescence (Zenit et al., 2001), and the velocity can be increased substantially by providing a direct impingement jet of water onto the bubble generator. Due to the rather large bubbles created by the bubble generator used in this apparatus, the creation of the smaller bubbles conducive to ignition were most likely generated as a result of the acoustic cavitation process which breaks larger bubbles into successively smaller ones until they are small enough to undergo CIBC.

Figure 16 shows the measured CO emissions data for propane-air bubbles in water. Here, propane was used as the fuel because it is inherently easier to burn than methane. A mixture of propane air with an equivalence ratio of $\phi = 0.95$ and $\phi = 1.27$ was injected into the system with a water flow rate of 1.0 liter · min^{-1} through a 9.5 mm anvil gap. Approximately 50 W of acoustic power was delivered to the probe tip to produce cavitation. From figure 16 we can see that upon the introduction of the propane gas, the generation of CO is immediately visible and steadily climbs and then exponentially levels off. This effect is a result of the time required to fill the void space (approx. 4 liter) above the liquid sump tank. At about 90 minutes, the acoustic power was increased to about 100 W, and we immediately see that this makes the rate of CO production increase. The CO levels continue to rise, and at about 110 minutes, we increase the equivalence ratio to $\phi = 1.27$. Again, we see the CO emissions rise as a result of more CO being generated at fuel-rich equivalence ratios compared to fuel-lean, and reach a peak value of about 160 ppm (2.5 ppm accuracy). At about 120 minutes, the acoustic horn suffers overheating and the power output drops resulting in a reduced CO emissions. Clearly, there is a direct correlation between the acoustic cavitation and the production of CO. As shown in figure 17, the measurement of CO production and how it tracks acoustic power or acoustic pressure amplitude is consistent with the computer model of CIBC.

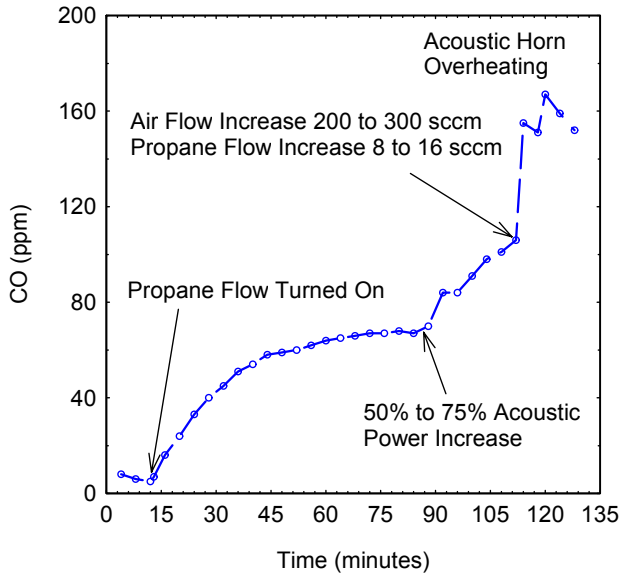

Figure 16.—Experimental data showing the production of CO as a function of time for propane-air bubbles in water with acoustic cavitation. The water flow rate was 1.0 liter/min through a 9.5 mm wide anvil gap. Note that a 75 percent acoustic power setting corresponds to approximately 100 W of acoustic power delivered at the probe tip. The equivalence ratio was set at $\phi = 0.95$ initially and increased to $\phi = 1.27$.

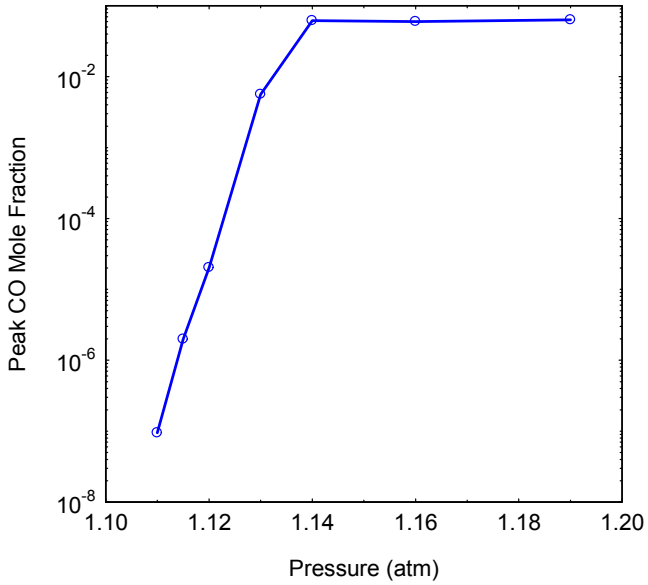

Figure 17.—Results from the computer model of CIBC showing the production of CO as a function of acoustic pressure (20 kHz) for a 4.5 μm radius methane-air (ϕ = 1.0) bubble in water.

We finally examine the effect of sonication on air bubbles in a hydrocarbon liquid. We use methanol as the liquid for the previously stated reasons, and flow it through the apparatus with conditions similar to water. However, we decreased the temperature of the methanol by using the chiller in order to reduce the effect of methanol vapor evaporation and condensation on the gaseous sampling line. At a temperature of 15 °C, the saturation properties of methanol in air result in a bubble with an equivalence ratio of 0.67. Although this is a fuel-lean case at the liquid temperature, it is expected that the higher temperatures inside the bubble will produce a more fuel-rich bubble prior to the time of ignition. We were not able to simulate the methanol-air bubble using the computer model due to the lack of a chemical kinetic mechanism for methanol-air chemistry. However, the experiment yields a result similar to the data acquired for propane-air bubbles in water. The important distinction here is that the fuel vapor is now provided by the working liquid and is not injected as a gas bubble. Figure 18 shows the experimental results of CIBC for air bubbles in methanol flowing at 1.0 liter · min^{-1} through a 9.5 mm anvil gap. Between 100 W and 140 W of acoustic power was delivered to the probe tip with a mixture of either air or a combination of argon-air. The use of argon generally provides higher adiabatic compression temperatures as indicated by earlier studies (Barber et al., 1997). From figure 18 we can see that as there is a definite correlation between the generation of CO and the acoustic power as the CO emissions drops towards zero when the acoustic power is cut off at about 130 minutes. The peak value of the CO (35 ppm) was less than the case using CH_4-air bubbles in water, and this can be partially attributed to the fuel-lean equivalence ratio (ϕ = 0.67) of the methanol-air mixture.

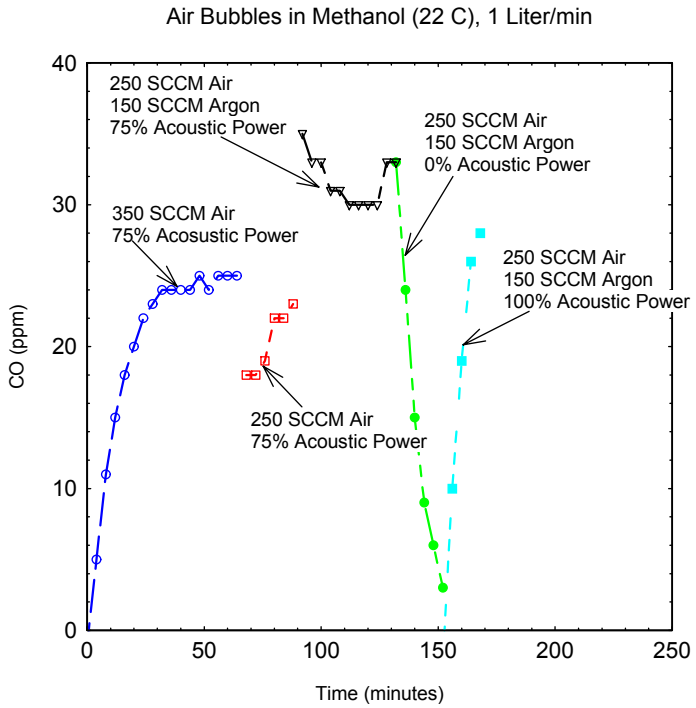

Figure 18.—Experimental data showing the production of CO as a function of time for air bubbles in methanol with acoustic cavitation. Methanol flow rate was 1.0 liter · min^{-1} through a 9.5 mm anvil gap. Methanol temperature was maintained at 15 C which provides a saturation equivalence ratio of $\phi = 0.67$.

Conclusions

The principle of using a collapsing bubble to effect ignition and combustion has been studied by both experiments and computational simulations of the cavitation-ignition bubble combustion (CIBC) process. A review of the literature related to hydraulic cavitation revealed that the micro-diesel effect (or the ignition of oil vapor mixtures within cavitating bubbles) has been known since the late 1960s.

For this study, we utilized ultrasonically induced cavitation (sonication) to initiate combustion in gaseous hydrocarbon-air bubbles in liquid water, and methanol vapor-air bubbles in liquid methanol. An ultrasonic cavitation flow reactor developed for this study provided a means of studying CIBC in a controlled manner with instrumentation and optical diagnostics. The apparatus provided a concentrated and uniform pressure field for acoustically exciting the two-phase flow that underwent cavitation. Visible light emission from CIBC was not found to provide any conclusive information regarding the existence of CIBC. The most conclusive proof of combustion came from the gaseous emission measurements: up to 160 ppm of carbon monoxide (CO) was found to be emitted as a byproduct of the gas-phase chemical reactions or combustion within the collapsing bubbles. The CO production occurred for both propane-air bubbles in water and for air bubbles in methanol, and was proportional to the acoustic power level delivered to the CIBC flow reactor.

In parallel with the experiments, we computationally modeled the CIBC process using a 1-D time-dependent compressible flow fluid dynamics code that included a comprehensive finite-rate chemical kinetics model. The computational model of the CIBC process indicated that gas-phase reactions within the bubble occurred and produced CO, CO_2, NO_X, and other gases. In addition, heat and mechanical

energy were released through a bubble volume expansion phase that occurs in the combusting bubble. The model showed that the CIBC process is sensitive to the fuel-air mixture ratio, the initial bubble diameter, the acoustic pressure forcing amplitude, and fluid properties. The results of the model were found to be consistent with the measured experimental results. In particular, the increase in the acoustic pressure (or sound intensity) resulted in a higher production of CO emissions.

For the simulations, we used a baseline case of 4.5 μm radius methane-air ($\phi = 1.0$) bubbles in liquid water undergoing a far-field acoustic pressure excitation of 1.19 atm at a frequency of 20 kHz. From this case we varied parameters such as far-field pressure, bubble radius, and equivalence ratio to examine their effects on bubble ignition and power output. Specifically, the model predicts that bubbles do not undergo ignition unless the internal bubble temperature reaches 2000 K, which corresponds to a far-field pressure of about 1.12 atm. The model also predicts that for a 20 kHz excitation frequency, the bubble diameters have to be within a certain size range (5 to 300 μm diameter for multiple acoustic cycle oscillations) in order for ignition to occur efficiently. This result is further restricted to bubbles smaller than 40 μm in diameter in the case of hydrodynamic cavitation as it occurs only once as a bubble passes through a pressure-dropping device such as an orifice. We also discovered that in order for net volume expansion work to be generated, the equivalence ratio must be greater than 0.5. Thus very fuel-lean mixtures cannot be used.

We found that in theory, it may be possible to develop a hydraulic-CIBC engine that produces net power using methane-air bubbles in water. The results of the model indicate that such a device, would require the following conditions to operate at a breakeven (self-sustaining mode): approximately 10 μm diameter methane-air bubbles in water, approximate $\phi = 1.25$, a liquid flow rate of at least 114 liter $\cdot$ min^{-1} (31 gal $\cdot$ min^{-1}) with a 10 percent bubble void fraction, a total pressure drop of less than 21 kPa (3 psid) provided by a venturi or other device with a pressure recovery factor of at least 85 percent, and no other losses in the device such as friction. Without the pressure recovery provided by the venturi, the hydraulic pump power required to provide conditions suitable for cavitation ignition is greater than the power that can be extracted from the resulting CIBC.

The above conclusions can be used as a basis to estimate the potential performance of a hydraulic-CIBC engine prototype that uses ATF as the working fluid. It is the opinion of the authors that such an engine prototype, in principle, may be able to produce net mechanical power if optimal flow conditions (low pressure drop), and optimal bubble ignition conditions (correct equivalence ratio control and bubble diameters) are satisfied, and an efficient power extraction process capable of harnessing the volumetric expansion work generated by the combusting bubble is developed.

References

B.P. Barber, R.A. Hiller, R. Lofstedt, S.J. Putterman, K. Weninger (1997), "Defining the unknowns of sonoluminescence", Physics Reports 281:65-143.

M.P. Brenner, S. Hilgenfeldt, D. Lohse (2002), "Single-bubble sonoluminescence," Rev. of Mod. Phys. 74:425-484.

H.-J. Lohrentz (1968), "Die Entwicklung etrem hoer Tempuraturen in Hydrauliksystemen und die Einflüsse dieser Temperaturen auf die Bauteile und ihre Funktion," Mineralötechnik, 13 Nr. 14/15.

J.M. Hobbs, D. McCloy (1972), "Cavitation Erosion in Oil Hydraulic Equipment," Metals and Materials, 1972, January, pp. 27-35.

G.E. Totten, Y.H. Sun, R.J. Bishop, X. Lin (1998), "Hydraulic System Cavitation: A Review," SAE International, Technical Paper Series 982036.

T.S. Koivula, A.U. Ellman (1998), "Cavitation Behavior of Hydraulic Orifices and valves," SAE International, Technical Paper Series 982038.

W. Backe, P. Lipphardht (1976), "Influence of Dispersed Air on the Pressure Medium," in Proc. Contamination of Fluid Power Systems, C97/76, p.77-84.

G.C. Svedberg, G.E. Totten, Y.H. Sun, R.J. Bishop, (1999) "Hydraulic System Cavitation: Part II – A Review of Hardware Design – Related Effects," SAE International, Paper 1999-01-2857.
D. Staeck (1987), "Gases in Hydraulic Oils," Tribologie & Schmierungstechnik 34(4):201-207.
R. Suzuki, Y. Tanaka, S. Yokota (1997), "Reduction of Oil Temperature Rise by Use of a Bubble Elimination Device in Hydraulic Systems," J. Soc. Trib. and Lubr. Eng. 54(3):23-27.
V.N. Likachev, G.S. Sukhov, L.P. Yarin (1992), "Towards a theory of Bubble Reactor Combustion Displacement Reactor," translated from Fizika Goreniya i Vzryva 28(2):24-31.
M.M. Carbonell, R. Giurardello (1997), "Modelling of a slurry bubble column reactor applied to the hydroconversion of heavy oils," Chem. Eng. Sci. 52(21/22):4179-4185.
V. Gol'dshtein, I. Goldfarb, I. Schrieber, A. Zinoviev (1998), "Oscillations in a combustible gas bubble," Comb. Theory Modelling 2:1-17.
M. Kitano, J. Shiba (1996), "Premixed Combustion of Liquid Fuel by Air Bubble Blowing," JSME International Journal B 39(4):844-850.
K.S. Suslick, Y. Didenko, M.M. Fang, T. Hyeon, K. Kolbeck, W.B. McNamara, M.M. Mdleneni, M. Wong (1999), "Acoustic cavitation and its chemical consequences," Phil. Trans. R. Soc. Lond. A 357:335-353.
K.S. Suslick, M.M. Mdleleni, J.T. Ries (1997), "Chemistry Induced by Hydrodynamic Cavitation," J. Am. Chem. Soc. 119:9303-9304.
A.B. Pandit, P. Senthil Kumar, M. Siva Kumar (1999), "Improve Reactions with Hydrodynamic Cavitation," Chem. Eng. Prog., May 1999
C. Gong, D.P. Hart (1998), "Ultrasound induced cavitation and sonochemical yields," J. Acoust. Soc. Am. 104(5):2675-2682.
C. Gong, D.P. Hart (1999), "Interactions of bubble dynamics and chemistry in cavitation bubbles induced by ultrasound," Proc. of the 3rd ASME/JSME Joint Fluids Eng. Conf., July 18-23, 1999, San Francisco.
A.J. Colussi, L.K. Weavers, M.R. Hoffmann (1998), "Chemical Bubble Dynamics and Quantitative Sonochemistry," J. Phys. Chem. A 102:6927-6934.
B.D. Storey, A.J. Szeri (1999), "Mixture segregation within sonoluminescing bubbles," J. Fluid Mech. 396:203-221.
V.Q. Vuong, A.J. Szeri, D.A. Young (1999), "Shock formation within sonoluminescence bubbles," Phys. Fluids 11(1):10-17.
A. Prosperetti, and A. Lezzi (1986), "Bubble dynamics in a compressible liquid. Part 1. First-order theory," J. Fluid Mech., 168:457-478.
L. Yuan, H. Y. Cheng, M.-C. Chu, P. T. Leung (1998), "Physical parameters affecting sonoluminescence: A self-consistent hydrodynamic study," Phys. Rev. E. 57:4265-4280.
R.J. Kee, F.M. Rupley, J.A. Miller (1989), "CHEMKIN II: A Fortran Chemical Kinetics Package for the Analysis of Gas-Phase Chemical Kinetics," Sandia Report SAND89-8009.
C.T. Bowman, R.K. Hanson, D.F. Davidson, W.C. Gardiner, Jr., V. Lissianski, G.P. Smith, D.M. Golden, M. Frenklach and M. Goldenberg, GRIMech 2.11 methane-air mechanism, http://www.me.berkeley.edu/gri_mech/
J.M. Hobbs, A. Laird (1969), "Pressure, temperature and gas content effects in the vibratory cavitation test," National Engineering Lab, Glasgow (Scotland), Properties of Fluids Div., available from www.ntis.gov, NTIS doc. N7110096.
J.M. Hobbs, D. Rachman (1970), "Environmentally Controlled Cavitation Test (Improvements in a Cavitating Film Erosion Test)," Characterization and Determination of Erosion Resistance, ASTM STP 474, American Society for Testing Materials, 1970, 29-47.
C.A. Wakeford, R. Blackburn, P.D. Lickiss (1998), "Effect of ionic strength on the acoustic generation of nitrite, nitrate and hydrogen peroxide," Ultrasonics Sonochemistry 6:141-148.
The Lee Co. (1997), Technical Hydraulic Handbook, Release 10.1, 1997, The Lee Co., P.O. Box 424, Westbrook, CT, 06498, p. M18.
R.C. Baker (2000), Flow Measurement Handbook, Cambridge Univ. Press, Cambridge, U.K., p. 99.

H. Hu, Z. Zhou, Z. Xu, J.A. Finch (1998), "Numerical and Experimental Study of a Hydrodynamic Cavitation Tube," Met. and Mat. Trans. B 29B:911-917.
C. England (1986), "Gas Solubilities in Physical Solvents," Chem. Eng., April 28, 1986, p.63-66.
J. Kojima and Q.V. Nguyen (2004), "Measurement and Simulation of Spontaneous Raman Scattering Spectra in High-Pressure, Fuel-Rich H_2-Air Flames," Meas. Sci. Tech., 15:565-580.
S.C. Chuang, V.W. Goldschmidt (1970), "Bubble Formation Due to a Submerged Capillary Tube in Quiescient and Coflowing Streams," ASME J. Basic Eng., Dec. 1970, p. 705-711.
R. Zenit, D.L. Koch, A.S. Sangani (2001), "Measurements of the average properties of a suspension of bubbles rising in a vertical channel," J. Fluid. Mech. 429:307-342.

DOE F 1332.1
(11-84)

U.S. DEPARTMENT OF ENERGY
REPORTING REQUIREMENTS CHECKLIST

FORM APPROVED
OMB NO. 1900-1401

1. PROGRAM/PROJECT TITLE
Cavitation-Ignition Bubble Combustion Study

2. IDENTIFICATION NUMBER
DE-AI05-02OR22929

3. PARTICIPANT NAME AND ADDRESS
NASA – John Glenn Research Center
Lewis Field
21000 Brookpark Road
Cleveland, Ohio 44135

4. PLANNING AND REPORTING REQUIREMENTS

	Frequency
A. General Management	
[ ] Management Plan	
[ ] Status Report	
[ ] Summary Report	
B. Schedule/Labor/Cost	
[ ] Milestone Schedule/Plan	
[ ] Labor Plan	
[ ] Facilities Capital Cost of Money Factors Computation	
[ ] Contract Facilities Capital and Cost of Money	
[ ] Cost Plan	
[ ] Milestone Schedule/Status	
[ ] Labor Management Report	
[ ] Cost Management Report	
C. Exception Reports	
[ ] Conference Record	
[ ] Hot Line Report	
D. Performance Measurement	
[ ] Management Control System Description	
[ ] WBS Dictionary	
[ ] Index	
[ ] Element Definition	
[ ] Cost Performance Reports	
[ ] Format 1 - WBS	
[ ] Format 2 - Function	
[ ] Format 3 – Baseline	

	Frequency
E. Financial Incentives	
[ ] Statement of Income and Expense	
[ ] Balance Sheet	
[ ] Cash Flow Statement	
[ ] Statement of Changes in Financial Position	
[ ] Loan Drawdown Report	
[ ] Operating Budget	
[ ] Supplementary Information	
F. Technical	A
[X] Notice of Energy RD&D Project (Required with any of the following)	
[X] Technical Progress Report	B
[ ] Draft for Review	
[ ] Final for Approval	
[ ] Topical Report	
[X] Final Technical Report	F
[ ] Draft for Review	
[X] Final for Approval	
[ ] Software	
[ ] Other (Specify)	

5. FREQUENCY CODES

A - As Required
B – Bi-Monthly
C - Change to Contractual Agreement
F - Final (end of effort)
M - Monthly
O - Once After Award
Q - Quarterly
S – Semi-Annually
X - With Proposal/Bid/Application or with Significant Changes
Y - Yearly or Upon Renewal of Contractual Agreement

6. SPECIAL INSTRUCTIONS (ATTACHMENTS)

[X] Report Distribution List/Addressees
[ ] Reporting Elements
[ ] Due Dates
[ ] Analysis Thresholds
[ ] Work Breakdown Structure
[ ] Other

7. PREPARED BY (SIGNATURE AND DATE)

8. REVIEWED BY (SIGNATURE AND DATE)

CONTRACT NUMBER:
DE-A105-02OR 22929

ADDRESSEES	[ ] Management Plan	[ ] Milestone Schedule & Status Report	[ ] Cost Plan	[ ] Manpower Plan	[ ] Contract Management Summary Report	[ ] Project Status Report	[ ] Cost Management Report	[ ] Manpower Management Plan	[ ] Conference Record	[ ] Hot Line Report	[ ] Notice of Energy RD&D Project (DOE F 1430.22)	[X] Technical Progress Report	[ ] Topical Report	[X] Final Technical Report	[ ]	[ ]	SPECIAL INSTRUCTIONS
	NUMBER OF REPORT COPIES																
Dr. James Conklin MS 6472 Oak Ridge National Laboratory 2360 Cherahala Blvd. Knoxville, TN 37932-6472												1		1			
Mary H. Rawlins Wayne Lin, LM-12 U.S. Department of Energy P.O. Box 2001 Oak Ridge, TN 37831-8759												1		1			
Walker K. Love U.S. Department of Energy Environmental Acquisitions Braach, AD-423 P.O. Box 2002 Oak Ridge, TN 37831-8759												1		1			

REPORT DOCUMENTATION PAGE

Form Approved
OMB No. 0704-0188

1. AGENCY USE ONLY (*Leave blank*)	2. REPORT DATE	3. REPORT TYPE AND DATES COVERED
	August 2005	Technical Memorandum

4. TITLE AND SUBTITLE

A Study of Cavitation-Ignition Bubble Combustion

5. FUNDING NUMBERS

WBS–22R–722–96–0224–03

6. AUTHOR(S)

Quang-Viet Nguyen and David A. Jacqmin

7. PERFORMING ORGANIZATION NAME(S) AND ADDRESS(ES)

National Aeronautics and Space Administration
John H. Glenn Research Center at Lewis Field
Cleveland, Ohio 44135–3191

8. PERFORMING ORGANIZATION REPORT NUMBER

E–15066

9. SPONSORING/MONITORING AGENCY NAME(S) AND ADDRESS(ES)

National Aeronautics and Space Administration
Washington, DC 20546–0001

10. SPONSORING/MONITORING AGENCY REPORT NUMBER

NASA TM—2005-213599

11. SUPPLEMENTARY NOTES

Responsible person, Quang-Viet Nguyen, organization code RTB, 216–433–3574.

12a. DISTRIBUTION/AVAILABILITY STATEMENT

Unclassified - Unlimited
Subject Categories: 23, 25, 28, 64, 70, 71, and 77

Available electronically at http://gltrs.grc.nasa.gov

This publication is available from the NASA Center for AeroSpace Information, 301–621–0390.

12b. DISTRIBUTION CODE

13. ABSTRACT ***(Maximum 200 words)***

We present the results of an experimental and computational study of the physics and chemistry of cavitation-ignition bubble combustion (CIBC), a process that occurs when combustible gaseous mixtures are ignited by the high temperatures found inside a rapidly collapsing bubble. The CIBC process was modeled using a time-dependent compressible fluid-dynamics code that includes finite-rate chemistry. The model predicts that gas-phase reactions within the bubble produce CO and other gaseous by-products of combustion. In addition, heat and mechanical energy release through a bubble volume-expansion phase are also predicted by the model. We experimentally demonstrate the CIBC process using an ultrasonically excited cavitation flow reactor with various hydrocarbon-air mixtures in liquid water. Low concentrations (< 160 ppm) of carbon monoxide (CO) emissions from the ultrasonic reactor were measured, and found to be proportional to the acoustic excitation power. The results of the model were consistent with the measured experimental results. Based on the experimental findings, the computational model, and previous reports of the "micro-diesel effect" in industrial hydraulic systems, we conclude that CIBC is indeed possible and exists in ultrasonically- and hydrodynamically-induced cavitation. Finally, estimates of the utility of CIBC process as a means of powering an idealized heat engine are also presented.

14. SUBJECT TERMS	15. NUMBER OF PAGES
Cavitation flow; Combustion chemistry; Bubbles; Fuels; Kinetics; Mathematical models	34
	16. PRICE CODE

17. SECURITY CLASSIFICATION OF REPORT	18. SECURITY CLASSIFICATION OF THIS PAGE	19. SECURITY CLASSIFICATION OF ABSTRACT	20. LIMITATION OF ABSTRACT
Unclassified	Unclassified	Unclassified	